

# Extractive-Catalytic Oxidative Desulfurization with Graphene Oxide-Based Heteropolyacid Catalysts: Investigation of Affective Parameters and Kinetic Modeling

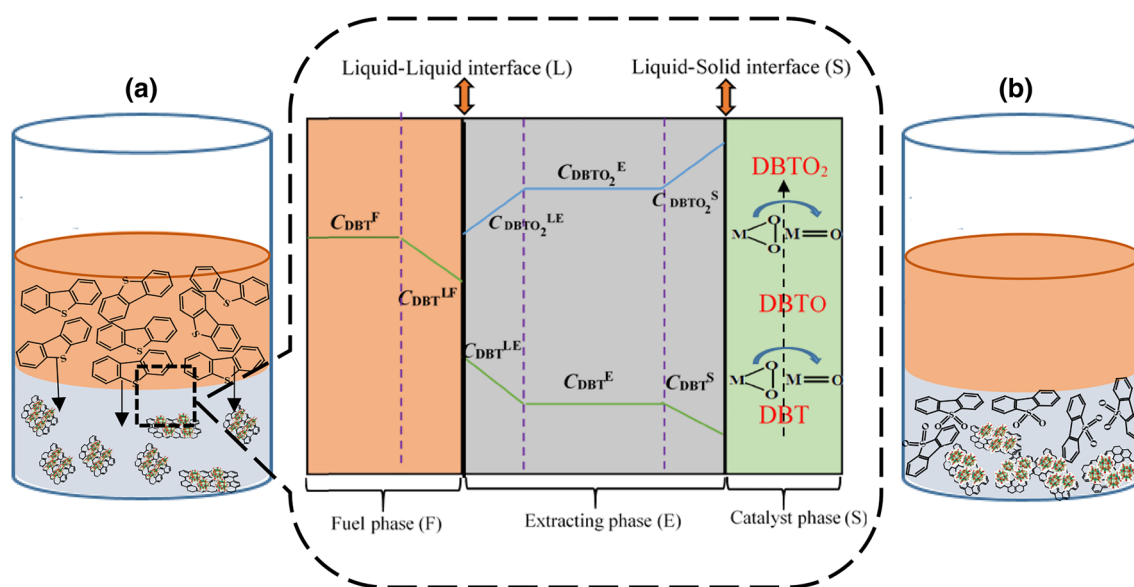
Azam Khodadadi Dizaji<sup>1</sup> · Hamid Reza Mortaheb<sup>1</sup> · Babak Mokhtarani<sup>1</sup>

Received: 1 September 2018 / Accepted: 13 October 2018 / Published online: 2 November 2018  
© Springer Science+Business Media, LLC, part of Springer Nature 2018

## Abstract

Different tungsten and molybdenum containing heteropolyacid (HPA) catalysts ( $H_3PMo_{12}O_{40}:Mo_{12}$ ,  $H_3PMo_8W_4O_{40}:Mo_8W_4$ ,  $H_3PMo_6W_6O_{40}:Mo_6W_6$ ,  $H_3PW_{12}O_{40}:W_{12}$ ) were immobilized on graphene oxide (GO) to obtain HPA–GO heterogeneous catalysts ( $Mo_{12}$ –GO,  $Mo_8W_4$ –GO,  $Mo_6W_6$ –GO, and  $W_{12}$ –GO). The synthesized catalysts were applied in removal of sulfur containing compounds [benzothiophene (BT), dibenzothiophene (DBT), and 4,6-dimethyldibenzothiophene (4,6-DMDBT)] with combined extraction–oxidation process using a batch reactor. The sulfur removal efficiency was gradually increased with increasing the ratio of molybdenum ions in the HPAs and complete sulfur removal efficiency for DBT was obtained for  $Mo_{12}$ –GO. The roles of affecting parameters such as extracting solvent, catalyst calcination, and feed concentration were also investigated. Among different extracting solvents including acetonitrile, DMF, NMP, methanol, water, and ethylene glycol, acetonitrile represented the best ECOD performance as the extracting solvent. The performance of non-calcined catalyst for sulfur removal was slightly better than that by the calcined one. It was also found that the high sulfur removal activity of the extractive-catalytic oxidative process (ECOD) was retained even at high feed concentration. The kinetic model was evaluated considering mass transfer coupled with chemical reaction, in which the catalytic oxidation reaction was recognized as the rate-controlling step. The kinetic parameters such as rate constants and apparent activation energy were determined.

## Graphical Abstract



**Keywords** Extractive-oxidative desulfurization · Graphene oxide · Heteropolyacids (HPAs) · Kinetic modeling · Mass transfer

## 1 Introduction

Emission of harmful exhaust gases from combustion of fuels containing sulfur compounds makes deep desulfurization as a crucial task [1, 2]. According to Euro V standard protocol, the maximum sulfur level should not exceed from 10 ppm in the diesel fuel [3].

The traditional hydrodesulfurization (HDS) is currently employed in purification of fuels [4, 5]. Although HDS can remove various S-compounds such as thiols, sulfides, and disulfides, it demands severe operating conditions i.e. high temperature and high hydrogen pressures for less reactivate heterocyclic thiophenic compounds such as dibenzothiophene (DBT) and its derivatives. Therefore, the development of new alternative or supplementary desulfurization technologies for production of clean fuels has become a huge challenge.

Recently, oxidation processes in different catalytic and non-catalytic forms have been increased as promising methods for removal of the aromatic sulfur compounds that are hardly eliminated by HDS [6–9].

Among the ODS processes, extractive catalytic oxidative desulfurization (ECOD) carried out in a biphasic system, is considered as one of the most promising methods with high commercialization potentials due to advantages such as operating at atmospheric pressure and low temperatures, simultaneous reaction and separation of sulfur compounds in a single unit, no adsorption of sulfone on the catalyst, and no need to strong stirring and complicated equipments [10–12]. In the ECOD process, sulfur containing compounds are catalytically oxidized to sulfones in a mild condition and sulfones are separated by adsorption, extraction, and distillation methods [13–15]. Among different catalysts used in the ECOD, heteropolyacids (HPAs) catalyst especially Mo- and W-based ones have stimulated much research activities due to their inherent redox potentials, acidities, and their stabilities [4]. Although there are many kinds of HPAs, Keggin structures are the most widely investigated ones because of their stabilities and ease of synthesis [16].

HPAs catalysts can be applied in homogeneous ways, however, problematic catalyst recovery inspires researchers to incorporate these active species on various solid supports such as  $\text{SiO}_2$ ,  $\text{Al}_2\text{O}_3$ , MOFs, CNT, and activated carbon to increase their reusability [6]. Meanwhile, those catalysts frequently suffer from a drawback of weak interaction between HPAs and the support leading to consequent leaching that makes these catalysts impractical for a continuous industrial application [3, 6, 15].

Nowadays, graphene-related materials have attracted great attention as novel catalyst supports due to their outstanding structural, physical, and chemical properties [5, 17]. Zhang and Wang claimed that GO has a high compatibility with the oxidative-adsorptive desulfurization system [18]. Menzel et al. applied GO-containing hybrids for adsorption of sulfur containing compounds from liquid hydrocarbons [19]. Hajjar and coworkers reported Co–Mo/graphene as an active HDS catalyst [20].

In our previous studies, GO supported HPAs as novel oxidation catalysts were introduced for the ECOD process and the optimum conditions of catalyst synthesis and operating condition were determined [6, 21]. The features such as rapid and complete ECOD desulfurization performance as well as high durability of the catalyst inspired us to investigate other effective parameters in the process.

Therefore, in the present research, several HPAs catalysts including  $\text{H}_3\text{PMo}_{12}\text{O}_{40}:\text{Mo}_{12}$ ,  $\text{H}_3\text{PMo}_8\text{W}_4\text{O}_{40}:\text{Mo}_8\text{W}_4$ ,  $\text{H}_3\text{PMo}_6\text{W}_6\text{O}_{40}:\text{Mo}_6\text{W}_6$ ,  $\text{H}_3\text{PW}_{12}\text{O}_{40}:\text{W}_{12}$  were immobilized on the graphene oxide (GO) to produce HPA–GOs heterogeneous catalysts ( $\text{Mo}_{12}$ –GO,  $\text{Mo}_8\text{W}_4$ –GO,  $\text{Mo}_6\text{W}_6$ –GO, and  $\text{W}_{12}$ –GO) and utilized in the ECOD process.

In addition, the effects of other parameters (extracting solvent, calcination of catalyst, and feed concentration) were investigated and a kinetic model was developed for the ECOD process.

## 2 Materials and Methods

### 2.1 Materials

Materials used in the present research including pristine graphite powder (Timcal, 325 mesh, 99.9%), phosphoric acid (Sigma-Aldrich, 99%), sulfuric acid (Merck, 98%), hydrochloric acid (Merck, 37%), hydrogen peroxide (Merck, 30% in water), sodium nitrate (Sigma-Aldrich, 99.8%), potassium permanganate (Merck, 99.5%), benzothiophene (BT, Merck, 99%), dibenzothiophene (DBT, Merck, 98%), 4,6-dimethyldibenzothiophene (4,6-DMDBT, Haohua Industry Company Ltd., China,  $\geq 99\%$ ), ethyl acetate (Merck, 99%), hexadecane (Merck, 99%), *n*-hexane (Merck, 99%), acetonitrile (Merck, 99.5%), *n*-methyl-2-pyrrolidone (NMP, Merck, 99.5%), dimethylformamide (DMF, Merck, 99.8%), methanol (Sigma-Aldrich, 99.8%), and ethylene glycol (Sigma-Aldrich, 99.8%), phosphomolybdic acid hydrate (Sigma-Aldrich, 99%), phosphotungstic acid hydrate (Sigma-Aldrich, 99%) were purchased. The

tungsten-substituted molybdophosphoric acids were prepared in the lab according to procedures in literature [3].

## 2.2 Catalyst Preparation

Immobilization of catalysts on GO were performed according to previously described procedures [6, 21], and the heterogeneous catalysts were then characterized. Graphene oxide was synthesized according to the modified Hummer method as described in previous papers [22, 23]. For each catalyst preparation, a colloidal suspension of GO ( $20 \text{ g L}^{-1}$ ) was sonicated in a mixed solvent (water/methanol with volume ratio of 1:1). Then equal mole content (0.001) of the HPA ( $\text{H}_3\text{PMo}_{12}\text{O}_{40}:\text{Mo}_{12}$ ,  $\text{H}_3\text{PMo}_8\text{W}_4\text{O}_{40}:\text{Mo}_8\text{W}_4$ ,  $\text{H}_3\text{PMo}_6\text{W}_6\text{O}_{40}:\text{Mo}_6\text{W}_6$ ,  $\text{H}_3\text{PW}_{12}\text{O}_{40}:\text{W}_{12}$ ) was added to the suspension. The containing vessel was kept under constant stirring (500 rpm) overnight on a magnetic stirrer at room temperature. After evaporating the mixtures solvent in a vacuum rotary evaporator ( $90^\circ\text{C}$ , 700 rpm), the mixture was dried at  $100^\circ\text{C}$  for 12 h. The dried solid was crushed in an agate mortar to obtain a powder as a HPA-GOs heterogeneous catalyst ( $\text{Mo}_{12}\text{-GO}$ ,  $\text{Mo}_8\text{W}_4\text{-GO}$ ,  $\text{Mo}_6\text{W}_6\text{-GO}$ , and  $\text{W}_{12}\text{-GO}$ ) and utilized in the ECOD process. For investigation of the calcination impact on the catalyst performance, a portion of the catalyst was calcined at  $300^\circ\text{C}$  for 3 h.

## 2.3 Characterization Analysis

FT-IR characterization of the samples was recorded by a Perkin-Elmer spectrum 65 frontier instrument (Germany). Energy dispersive spectroscopy (EDS) was taken to determine the elemental analysis (EDX, TESCAN, Vega3, Czech Republic). The sulfur content analyses were made with a gas chromatograph (GC, Varian, CP-3800) with a flame ionization detector (FID) and capillary column (Chrompack,  $30 \text{ m} \times 0.25 \text{ mm} \times 1.2 \mu\text{m}$ ). The GC analysis conditions were as follows: carrier gas of nitrogen; injector temperature,  $280^\circ\text{C}$ ; detector temperature,  $280^\circ\text{C}$ ; column temperature,  $200^\circ\text{C}$  for 2 min, and then heated to  $280^\circ\text{C}$  for 15 min with a rate of  $10.0^\circ\text{C min}^{-1}$ . Hexadecane was used as the internal standard.

## 2.4 Experimental Methods

Batch experiments were conducted in a 100-mL round-bottom flask immersed in an oil bath placed on a mechanical stirrer. Various model fuels were prepared by dissolving different amounts of sulfur containing compounds (BT, DBT, and 4,6-DMDBT) in *n*-hexane (500 ppmw).

A water condenser was fixed on the middle neck of the flask and the side neck was plugged with a stopper. A comparison between performances of the prepared catalysts was carried out in the oxidation of different sulfur containing compounds (BT, DBT, and 4,6-DMBT) with a model fuel (500 ppmw), an oxidant/sulfur molar ratio (O/S) of 6, and  $E/F = 0.3$  at  $50^\circ\text{C}$  for 30 min.

Different extracting solvents namely acetonitrile, DMF, NMP, methanol, water, and ethylene glycol were used to assess the effect of extracting solvent.

The solvent used in the experiment containing  $\text{DBTO}_2$  is then distilled in a distillation column, in which  $\text{DBTO}_2$  is separated from the solvent at the bottom of the column and the distilled solvent as the top product is recycled to the process.

After the oil bath was heated up to the desired temperature, the required amounts of catalyst (0.1 mol), hydrogen peroxide ( $O/S = 6$ ), with a constant volumetric ratio of the extracting solvent to the model fuel (1.5 mL/5 mL) were added to the flask. The suspension was then stirred continually and vigorously with a constant speed of 500 rpm. The samples were periodically withdrawn from the fuel phases during the reaction, and the sulfur contents were analyzed by the GC-FID. The volumes of reaction mixtures were assumed constant due to small amounts of liquid samples ( $\sim 200 \mu\text{L}$ ).

The measurements were performed by injecting  $1 \mu\text{L}$  of the sample and hexadecane as the internal standard. Each experimental point was repeated at least two times.

The sulfur removal ( $R$ ) was calculated using initial sulfur concentration ( $C_0$ ) and the sulfur concentration at each time ( $C_t$ ) as follows:

$$R = \frac{C_{\text{DBT}}^0 - C_{\text{DBT}}^F}{C_{\text{DBT}}^0} \times 100(\%) \quad (1)$$

A pseudo first-order kinetic model (Eq. 2) and the Arrhenius equation (Eq. 4) were used in order to determine the kinetic rate constant and activation energy of the ECOD process.

$$r = -\frac{dC_{\text{DBT}}^F}{dt} = K_r'' C_{\text{DBT}}^F \quad (2)$$

$$\ln\left(\frac{C_{\text{DBT}}^F}{C_{\text{DBT}}^0}\right) = -K_r'' t \quad (3)$$

$$\ln K_r'' = \ln A - \frac{E_a}{RT} \quad (4)$$

in which,  $A$  is the pre-exponential factor,  $E_a$  represents the activation energy,  $T$  is the temperature ( $K''_r$ ), and  $R$  is the gas constant, respectively [15].

### 3 Results and Discussion

#### 3.1 Catalyst Characterization

A comprehensive characterization of the catalysts, which were synthesized based on the same procedure, were brought in our previous works [6, 21]. In the present work, the FTIR and EDX analyses of the synthesized catalysts are presented.

Figure 1 depicts the FT-IR spectra for different heteropolyacids before and after immobilization on GO. The four FT-IR characteristic bands detected around 1075, 975, 878, and 786  $\text{cm}^{-1}$  that demonstrate the Keggin type structure, are attributed to vibrations of  $\text{P-O}_a$ ,  $\text{M=O}_d$ ,  $\text{M-O}_b\text{-M}$ , and  $\text{M-O}_c\text{-M}$  ( $\text{M}=\text{W}, \text{Mo}$ ), respectively [3]. The presence of characteristic vibration bands of the synthesized catalyst

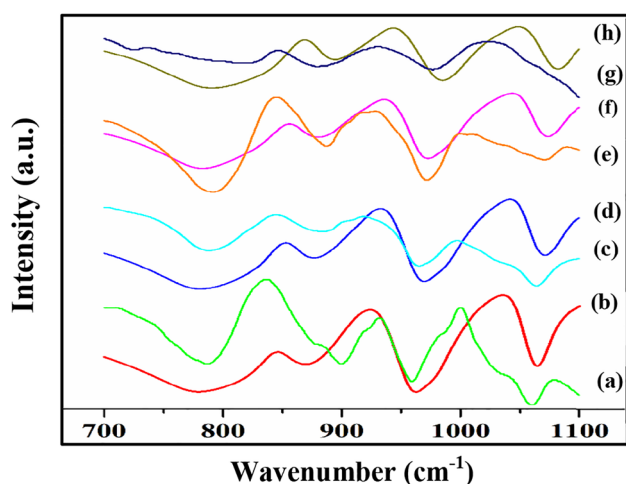


**Fig. 1** FTIR spectra of (a)  $\text{Mo}_{12}\text{-GO}$ , (b)  $\text{Mo}_{12}$ , (c)  $\text{Mo}_8\text{W}_4\text{-GO}$ , (d)  $\text{Mo}_8\text{W}_4$ , (e)  $\text{Mo}_6\text{W}_6\text{-GO}$ , (f)  $\text{Mo}_6\text{W}_6$ , (g)  $\text{W}_{12}\text{-GO}$ , and (h)  $\text{W}_{12}$

**Table 1** FT-IR data of  $\text{Mo}_{12}$ ,  $\text{Mo}_{12}\text{-GO}$ ,  $\text{Mo}_8\text{W}_4$ ,  $\text{Mo}_8\text{W}_4\text{-GO}$ ,  $\text{Mo}_6\text{W}_6$ ,  $\text{Mo}_6\text{W}_6\text{-GO}$ ,  $\text{W}_{12}$ , and  $\text{W}_{12}\text{-GO}$

Samples	Wavenumber ( $\text{cm}^{-1}$ )							
	P-O	Shift	M=O	Shift	M-O <sub>c</sub> -M	Shift	M-O <sub>b</sub> -M	Shift
$\text{Mo}_{12}$	1065	6	964	5	868	32	783	2
$\text{Mo}_{12}\text{-GO}$	1059		959		900		785	
$\text{Mo}_8\text{W}_4$	1071	7	970	8	871	11	783	
$\text{Mo}_8\text{W}_4\text{-GO}$	1064		962		882		788	5
$\text{Mo}_6\text{W}_6$	1071	3	971	0	871	20	781	12
$\text{Mo}_6\text{W}_6\text{-GO}$	1074		971		891		793	
$\text{W}_{12}$	1081	17	983	11	892	15	785	35
$\text{W}_{12}\text{-GO}$	1098		972		877		820	

as well as those of original HPA indicates that HPAs are present in the catalyst structure without any decomposition [13].

As seen in the Fig. 1, there are slight shifts in the positions of some characteristic bands after immobilization, which can be related to the electrostatic interaction between negatively charged HPAs and positively charged GO surface [6, 21]. At least a part of observed shifts in the IR spectra (Table 1) can be attributed to the changes of electron density or delocalized charge of HPA due to the electrostatic interactions between the HPA anion and the protonated surface functional groups [24].

Figure 2 represents the EDX spectra of HPA-GO heterogeneous catalysts. As shown in the Fig. 2 the presence of different elements (W, Mo, and P) with diverse intense in the corresponded EDX spectra confirms successful immobilization of different HPAs on GO support (carbon and oxygen come from GO support).

#### 3.2 Comparison of HPA-GO Catalysts Performances

As seen in Fig. 3, the order of sulfur removal for different sulfur compounds is:  $\text{DBT} > 4,6\text{-DMDBT} > \text{BT}$ . The reactivities of sulfur-containing compounds increase with increasing the electron density on the sulfur atoms. BT with the lowest electron density (5.696) compared to DBT (5.758) and 4,6-DMDBT (5.76) is supposed to have the lowest reactivity [18, 25]. Similar reactivities of DBT and 4,6-DMDBT could be attributed to their close electron densities as well as the suppressed steric hindrance of methyl groups in 4,6-DMDBT [26] due to flat nonporous surface of the catalyst.

Although all catalysts have high catalytic activities, the sulfur removal is gradually increased with replacement of tungsten by molybdenum atoms and  $\text{Mo}_{12}\text{-GO}$  catalyst has the highest activity among the investigated samples. Even though Molybdenum and Tungsten-based HPAs they belong to the same group in the periodic table, they have different catalytic activities and stabilities [27]. As reported by Okuhara [16], the O1s binding energy of HPA structure for

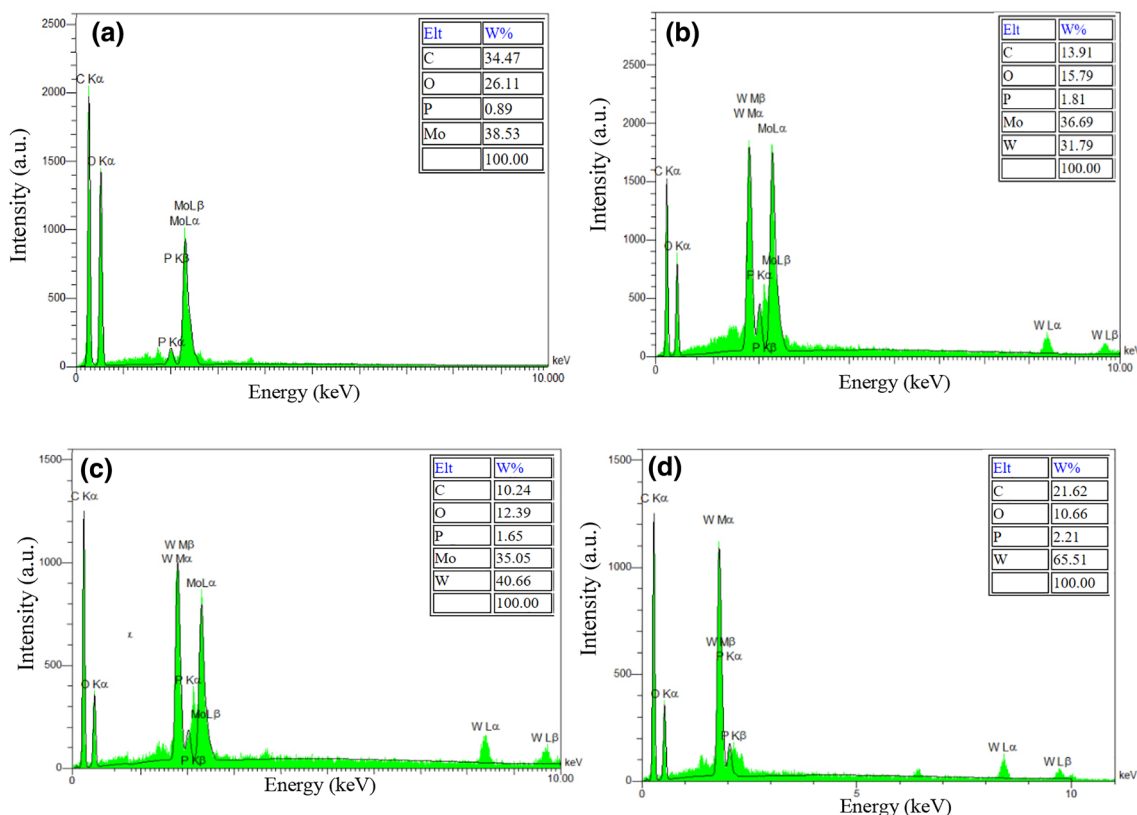


Fig. 2 EDX spectra of (a)  $\text{Mo}_{12}\text{-GO}$ , (b)  $\text{Mo}_8\text{W}_4\text{-GO}$ , (c)  $\text{Mo}_6\text{W}_6\text{-GO}$ , and (d)  $\text{W}_{12}\text{-GO}$

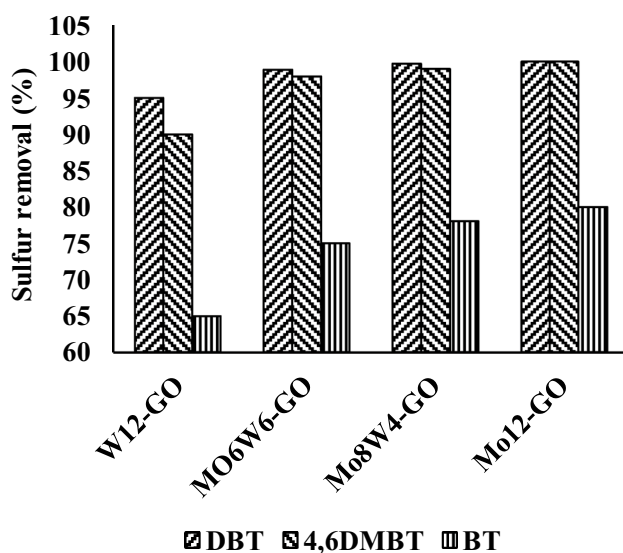


Fig. 3 ECOD of different sulfur containing compounds using various catalysts: experimental conditions:  $T=50\text{ }^\circ\text{C}$ ,  $\text{O/S}=6$ , extracting solvent: acetonitrile,  $\text{E/F}=0.3$ , sulfur containing compound: DBT, and 30-min run

tungstates is higher than that for molybdates. Furthermore, the extent of electron delocalization increases with increasing the number of molybdenum atoms in a Keggin structure. These might be the reasons that explain the highest catalytic activity of  $\text{Mo}_{12}\text{-GO}$  among the studied catalysts. The same results were reported by Choi et al. [28], in which molybdic compounds was found to have a higher oxidation potential as compared to tungstic compounds.

### 3.3 Effect of Extracting Solvent

In order to investigate the effect of different extracting solvent on the ECOD performance, different extracting solvents including NMP, DMF, acetonitrile, methanol, ethylene glycol, and  $\text{H}_2\text{O}$  were used. Firstly, the performances of different extracting solvents on removal of DBT were evaluated in extractive desulfurization process (Table 2). The order of sulfur elimination was  $\text{NMP} (88.2\%) > \text{DMF} (87.1\%) > \text{acetonitrile} (59.4\%) > \text{methanol} (39.7\%) > \text{ethylene glycol} (11.1\%) > \text{H}_2\text{O} (1.5\%)$ . Almost no DBT was extracted into water because of more polarity of water molecules than that of DBT [14].

**Table 2** Effect of different solvents in extractive desulfurization and ECOD process for removal of DBT

Extracting solvent	Sulfur removal by extractive desulfurization (%)	Nernst partition coefficients ( $K_N$ )	Sulfur removal by ECOD process (%)
NMP	88.2	7.47	99.4
DMF	87.1	6.75	98.9
Acetonitrile	59.4	1.46	100.0
Methanol	39.7	0.66	76.1
Ethylene glycol	11.1	0.12	27.0
H <sub>2</sub> O	1.5	0.02	–

Experimental conditions:  $T=50\text{ }^\circ\text{C}$ , catalyst ( $\text{Mo}_{12}\text{-GO}$ ) loading:  $2.4\text{ g L}^{-1}$ , extracting solvent: acetonitrile,  $E/F=0.3$ , sulfur containing compound: DBT,  $O/S=6$ , and 30-min run

The values of Nernst partition coefficients,  $K_N$ , which is defined as the ratio of sulfur concentration in the extractant phase,  $C_{\text{DBT,E}}$ , to the sulfur concentration in the fuel phase,  $C_{\text{DBT,F}}$ , in the extraction of DBT are also represented in Table 2 for different extracting solvents. As seen in the table, NMP and DMF have the highest Nernst partition coefficients. The similar results were also observed in previous studies [14, 29, 30]. Although high  $K_N$  values represent good extractive desulfurization efficiencies, there are problems in separation of oxidized compounds from these non-green solvents due to their high boiling points.

Nevertheless, in the ECOD systems, the order of DBT elimination is as follows: acetonitrile (100%) > NMP (99.4%) > DMF (89.3%) > methanol (76.1%) > ethylene glycol (27%) > H<sub>2</sub>O (0%) at 50 °C. The different trend between the result of sulfur elimination by the ECOD process and those by extraction with various extracting solvents (Table 2) suggests that the extraction process may not be the main contributor of sulfur elimination.

The highest performance of acetonitrile in the ECOD process might be related to aprotic property of acetonitrile [11, 30] as the nucleophilic oxidation reaction is performed better in the aprotic solvents with higher dielectric constants than in the protic solvents [14].

In addition, low surface tension of acetonitrile may facilitate the mass transfer between fuel and the extracting solvent by formation of smaller droplets and higher contact areas [12]. Besides, acetonitrile is chosen as a suitable solvent owing to its appropriate dissolution ability and low boiling point resulting in economical and cost-effective recovery of the extracting solvent [11, 31].

### 3.4 Effect of Catalyst Calcination

The sulfur removals in the ECOD process using non-calcined catalyst ( $\text{Mo}_{12}\text{-GO}$ ) and the calcined one at 300 °C are compared in Fig. 4. According to Fig. 4a, the non-calcined catalyst represents a slight higher sulfur removal than the calcined one.

By increasing the temperature up to 120 °C, physisorbed and interlamellar water molecules are firstly eliminated. Further increasing of temperature up to 200 °C will decompose the covalently bonded oxygen functional groups. Increasing temperature up to 300 °C will remove more stable oxygen containing functional groups [32].

According to Fig. 4b and the inset table, EDX analysis shows removal of some surface oxygen functional groups after calcination.

With comparing the calcined and non-calcined performance data of catalysts and the EXD analysis results, it may be concluded that the oxygen functional groups play a role in the catalytic performance of the catalyst. The result is in agreement with a study conducted by Gu et al. [33], in which the surface oxygen groups of a special carbocatalysis have been recognized as the active sites for oxidation of various substrates. Despite of a small difference between the performance of the calcined and non-calcined catalysts before 30 min, there is an insignificant difference between their ultimate performances.

As reported by Katheria et al. calcination can increase the interaction between the support and active catalytic species and improve the catalyst stability [34]. Taking into account the stability consideration, the calcined catalyst was selected to be used in the rest of experiments.

### 3.5 Effect of Feed Sulfur Concentration

Figure 5 compares the sulfur removals for the feeds with different concentrations. The same final sulfur removals of 100% were obtained within 30 min for the feeds having 200 and 500 ppmw sulfur contents. As the initial sulfur content is increased to 1000 ppmw, the final sulfur removal of 97.5% is obtained. Increase in the initial sulfur content from 200 to 500 ppmw can speed up the oxidation of DBT and meanwhile deepen the DBT removal with the law of mass action [4]. However, by further increasing of sulfur initial content, owing to the large amount of DBT and

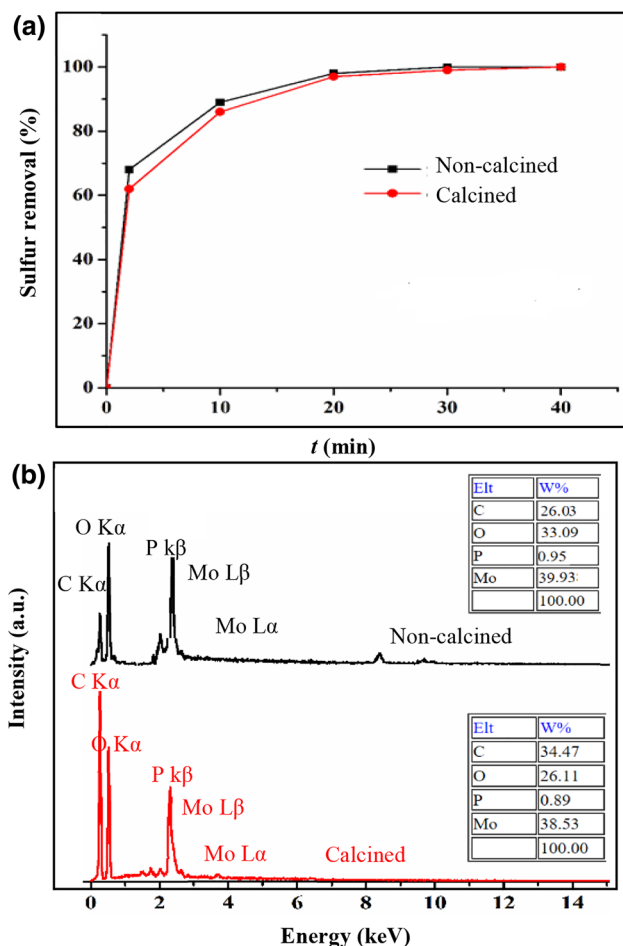


**Fig. 4** (a) Effect of calcination on catalyst performance, and (b) EDX analyses of calcined and non-calcined catalysts. Experimental conditions:  $T=50\text{ }^{\circ}\text{C}$ , Catalyst ( $\text{Mo}_{12}\text{-GO}$ ) loading:  $2.4\text{ g L}^{-1}$ ,  $\text{O/S}=6$ , extracting solvent: acetonitrile,  $\text{E/F}=0.3$ , sulfur containing compound: DBT, and 30-min run

limited capacity of the extracting solvent, the insufficient catalytic active sites can convert lower DBT [35]. Nevertheless, it is noticeable that ODS is usually considered as a complementary process for HDS, and thus for the feed concentrations around 500 ppm, in which the process represents a fast and complete removal.

### 3.6 Comparison of Catalyst Performances in Current and Previous Researches

Table 3 summarizes recently published ECOD data using molybdenum and tungsten containing heterogeneous catalysts as well as the results in the current research. As seen in the table, the results of current study represent superior performances in terms of sulfur removal, catalyst usage, and reaction time in moderate operating conditions (temperature and O/S ratio). While the conventional

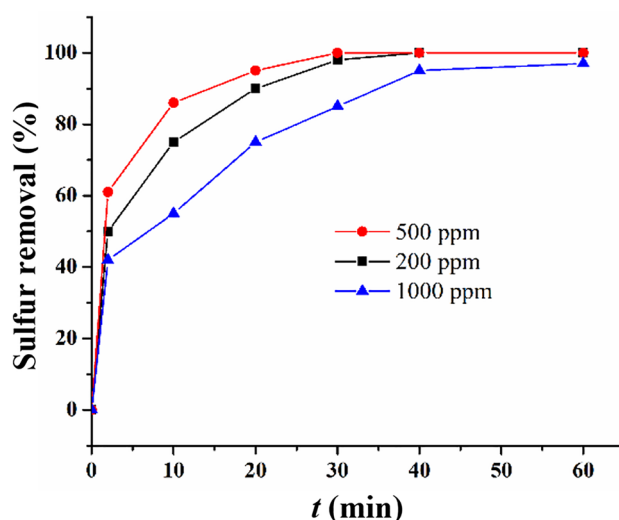


**Fig. 5** Effect of feed concentration on sulfur removal. Experimental conditions:  $T=50\text{ }^{\circ}\text{C}$ , Catalyst ( $\text{Mo}_{12}\text{-GO}$ ) loading:  $2.4\text{ g L}^{-1}$ ,  $\text{O/S}=6$ , extracting solvent: acetonitrile,  $\text{E/F}=0.3$ , sulfur containing compound: DBT, and 30-min run

heterogeneous catalysts suffer from slow diffusion rate of reactants through the pores of the catalyst, the superior performance of introduced catalysts in the current research can be partly attributed to the two-dimensional nonporous structure of the support with large specific surface area that not only provides abundant catalytic site for the reactants but also reduces the penetration resistance.

### 3.7 ECOD Modeling

The ECOD process is comprised of a mass transfer step (extraction) and a chemical reaction step (catalytic oxidation reaction) taking place simultaneously in a biphasic system consisting of a nonpolar phase (fuel) and a polar phase (extracting solvent). The sulfur containing compounds exist in the nonpolar phase whereas the oxidants and catalyst reside primarily in the polar phase. Initially,  $\text{H}_2\text{O}_2$  was adsorbed on the surface of the catalyst and the active polyoxoperoxy intermediates species are generated by nucleophilic attack of  $\text{H}_2\text{O}_2$  [13]. According to the GC analyses at consecutive time intervals (Fig. 6a), DBT is continuously diffused from the model fuel and simultaneously the extracted DBT is oxidized to the corresponding sulfone ( $\text{DBTO}_2$ ) (Fig. 6b). Since no DBTO was detected by the GC analysis, it is inferred that the intermediate product (DBTO) is quickly converted to  $\text{DBTO}_2$ . Finally, the strong polar  $\text{DBTO}_2$  is transferred from the catalytic surface into the extracting solvent and retains in the polar extracting phase owing to their similar polarities.

**Table 3** Comparison of ECOD results for molybdenum and tungsten containing heterogeneous catalysts

Entry	Catalyst	Extracting solvent	Sulfur (ppm)	Catalyst loading (g L <sup>-1</sup> )	T (°C)	O/S ratio (-)	t (min)	Sulfur removal (%)	Year	References
1	Mo <sub>12</sub> -GO	Acetonitrile	500	2.4	50	6	30	100	2018	This work
2	Mo <sub>8</sub> W <sub>4</sub> -GO	Acetonitrile	500	3	50	6	30	99.7	2018	This work
3	Mo <sub>6</sub> W <sub>6</sub> -GO	Acetonitrile	500	3.1	50	6	30	98.9	2018	This work
4	W <sub>12</sub> -GO	Acetonitrile	500	5.2	50	6	30	95	2018	This work
5	Mo-Al <sub>2</sub> O <sub>3</sub>	Acetonitrile	320	62.4	60	11	60	85	2008	[36]
6	Mo/γ-Al <sub>2</sub> O <sub>3</sub>	Acetonitrile	320	13	60	2.3	60	100	2015	[14]
7	Mo/γ-Al <sub>2</sub> O <sub>3</sub>	Acetonitrile	320	20	50	7	120	100	2016	[11]
8	HPW/Al <sub>2</sub> O <sub>3</sub>	Acetonitrile	350	4	60	8	120	99.2	2016	[37]
9	HPW/T-ER	Acetonitrile	330	5	333	5	240	84	2003	[38]
10	HPW/MIL	Acetonitrile	500	50	323	6	60	100	2013	[39]

### 3.7.1 Mass Transfer Modeling

As the two liquid phases are mixed together, transferring of DBT from the model fuel phase to the extracting phase is initiated due to vigorous agitation and relatively higher solubility of DBT in the extracting solvent. Based on the two-film theory, the DBT concentration profiles across the liquid-liquid and liquid-solid interfaces are established as shown in Fig. 7. DBT is transferred from the bulk of the model fuel ( $C_{DBT}^F$ ) to the liquid-liquid interface ( $C_{DBT}^{LF}$ ). It is then dissolved in the extracting phase ( $C_{DBT}^{LF}$ ) and transferred in the first liquid film toward the bulk of extracting phase ( $C_{DBT}^E$ ). A concentration gradient for DBT is established across the second liquid film inside the extraction phase and the liquid-solid interface ( $C_{DBT}^S$ ).

On the other hand, DBTO<sub>2</sub> is produced on the catalyst surface ( $C_{DBTO_2}^S$ ) and transferred across the second film toward the bulk of extracting phase ( $C_{DBTO_2}^E$ ). Because of low solubility of DBTO<sub>2</sub> in the model fuel, its concentration in the model fuel can be neglected. Mass transfer rates of DBT can be represented by the following equations:

$$j_{DBT}^F = k_F a_L (C_{DBT}^F - C_{DBT}^{LF}) \quad (5)$$

$$j_{DBT}^E = k_E a_L (C_{DBT}^{LE} - C_{DBT}^E) \quad (6)$$

$$C_{DBT}^{LE} = K_D C_{DBT}^{LF} \quad (7)$$

in which,  $K_D$  is the partition coefficient between the model fuel and the extracting phase assuming equilibrium at the L-interface.

$$j_{DBT}^S = k_S a_S (C_{DBT}^E - C_{DBT}^S) \quad (8)$$

$j_{DBT}^F$ ,  $j_{DBT}^E$ , and  $j_{DBT}^S$  are mass transfer rates of DBT in the model oil, extracting phase, and on the catalyst surface (mol m<sup>-3</sup> min<sup>-1</sup>), respectively.  $k_F$ ,  $k_E$ , and  $k_S$  are mass transfer coefficients for DBT (m min<sup>-1</sup>) in the model oil, and the two interfaces in the extracting phase, respectively.  $a_L$  and  $a_S$  are specific area of the liquid-liquid and liquid-solid interfaces (m<sup>2</sup> m<sup>-3</sup>), respectively [11].

It is noticeable that in the ECOD process, since H<sub>2</sub>O<sub>2</sub> is rapidly transferred to the catalyst active sites, the corresponding mass transfer resistance can be neglected.

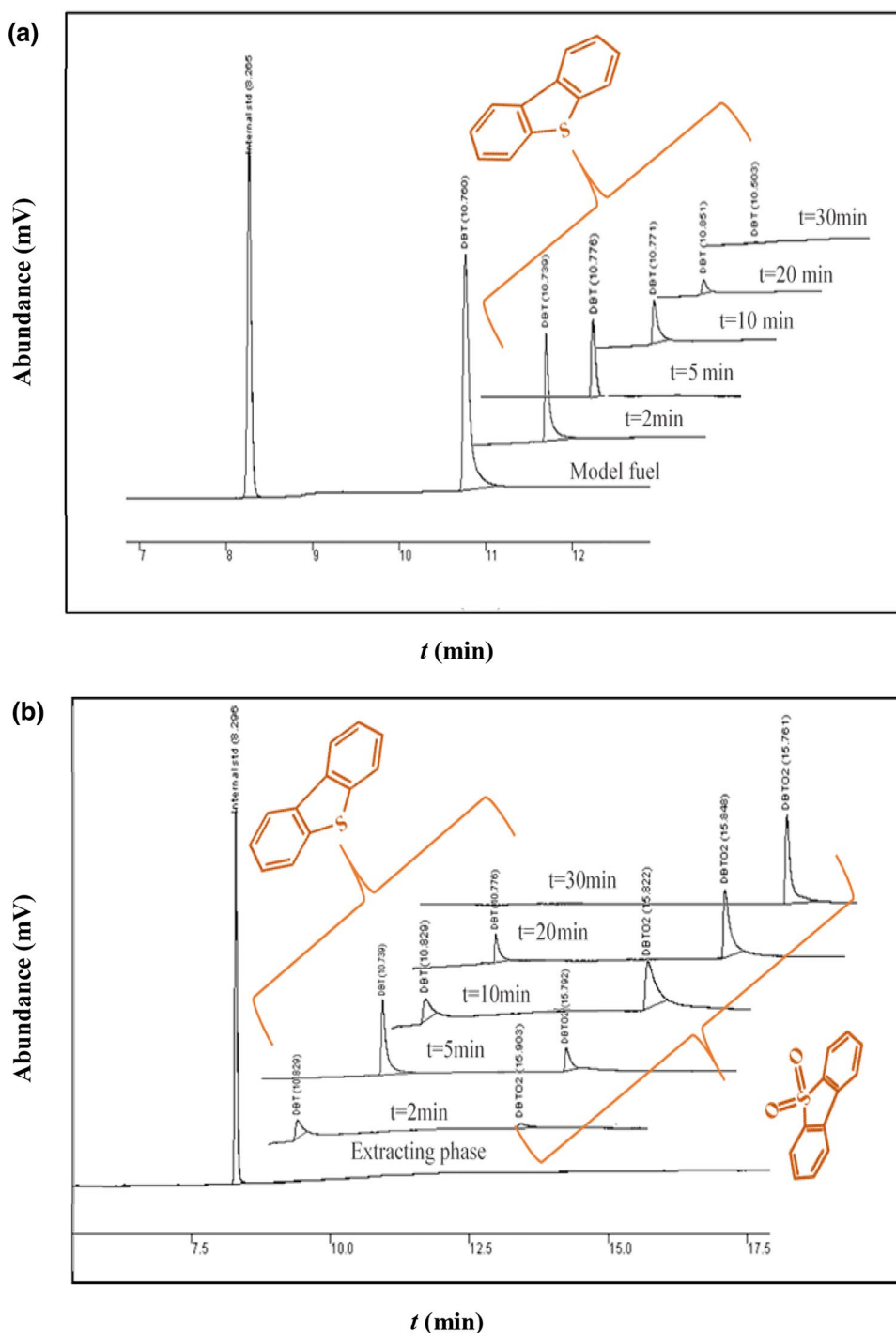
### 3.7.2 Heterogeneous Catalytic Reaction Modeling

Seven sequential steps are involved typically in a classical heterogeneous catalytic reaction i.e. (1) External diffusion including transferring of the reactants from the bulk phase to the external surface of the catalyst; (2) Internal diffusion including moving of the reactants inside the pores to vicinity of the active sites; (3) Adsorption of the reactants on the internal surface of the catalyst; (4) Reaction at definite active sites; (5) Desorption of the products from the inside surface of the catalyst; (6) Internal diffusion comprising diffusion of the products from the inner of the catalyst to its outer surface; and (7) External diffusion of the products from the external surface of catalyst to the fluid bulk [17, 40]. Therefore, the rate of heterogeneous catalytic reactions and their selectivity greatly depend on the penetration/mass transfer of the reactants.

Applying GO as the catalyst base will eliminate steps 2 and 6 in the mass transfer mechanism because of its non-porous nanostructure. Furthermore, GO can accelerate step 3 by assisting to the adsorption of reactants (DBT and H<sub>2</sub>O<sub>2</sub>) [6, 41]. Furthermore, acetonitrile as the extracting solvent with appropriate physiochemical properties accelerates steps 1 and 7 [11].



**Fig. 6** GC-FID spectra of (a) fuel phase, and (b) extracting phase at initial, and after 2, 5, 10, 20, and 30 min. Experimental conditions:  $T=50\text{ }^{\circ}\text{C}$ , Catalyst ( $\text{Mo}_{12}\text{-GO}$ ) loading:  $2.4\text{ g L}^{-1}$ ,  $O/S=6$ , extracting solvent: acetonitrile,  $E/F=0.3$ , sulfur containing compound: DBT, and 30-min run



An accepted two-step oxidation reaction sequence that leads to production of sulfoxide and sulfone and regeneration of the catalyst is represented in Fig. 8 [42] ( $k_1$ ,  $k_{-1}$ ,  $k_2$ , and  $k_3$  represent the reaction rate constants). The peroxomolybdate species ( $\text{MoO}_2$ ) are regenerated by reaction of the catalyst ( $\text{MoO}$ ) with  $\text{H}_2\text{O}_2$ .  $\text{MoO}_2$  reacts then with the adsorbed DBT to produce sulfoxide (DBTO) [11, 14]. A half-circle of reaction is then repeated and  $\text{MoO}_2$  is reproduced. The reproduced  $\text{MoO}_2$  reacts with DBTO to produce  $\text{DBTO}_2$  [7, 43,

44]. In the above mechanism, the oxygen transfer to DBT (oxidation of DBT to DBTO) is the rate-controlling step of the oxidation reaction [3, 36].

The rate of DBT oxidation to sulfoxide can be expressed by Eq. (9)

$$-r_{\text{DBT}} = -\frac{dC_{\text{DBT}}}{dt} = k_2 C_{\text{DBT}} C_{\text{MoO}_2} \quad (9)$$

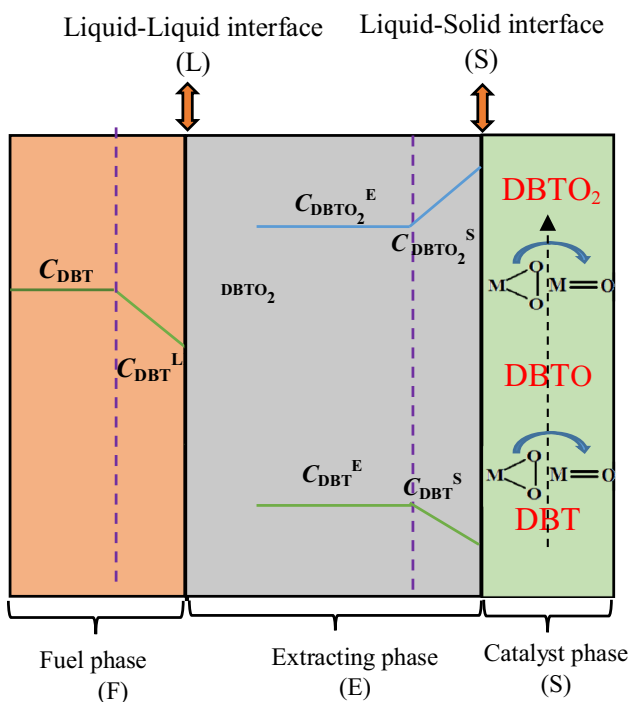


Fig. 7 Concentration profiles of DBT and sulfone during the ECOD process

Considering zero consumption rate of the intermediate activated catalyst species, the rate of MoO<sub>2</sub> consumption can be written as:

$$-r_{\text{MoO}_2} = \frac{dC_{\text{MoO}_2}}{dt} = 0 \tag{10}$$

$$k_1 C_{\text{MoO}} C_{\text{H}_2\text{O}_2} - k_{-1} C_{\text{MoO}_2} = k_2 C_{\text{MoO}_2} C_{\text{DBT}}^S + k_3 C_{\text{DBTO}_2}^S C_{\text{MoO}_2} \tag{11}$$

$$C_{\text{Mo}} = C_{\text{MoO}_2} + C_{\text{MoO}} \tag{12}$$

From Eq. (11) and the mass balance (Eq. 12), the C<sub>MoO<sub>2</sub></sub> can be given by Eq. (13):

$$C_{\text{MoO}_2} = \frac{k_1 C_{\text{Mo}} C_{\text{H}_2\text{O}_2}}{k_{-1} + k_2 C_{\text{DBT}}^S + k_1 C_{\text{H}_2\text{O}_2} + k_3 C_{\text{DBTO}_2}^S} \tag{13}$$

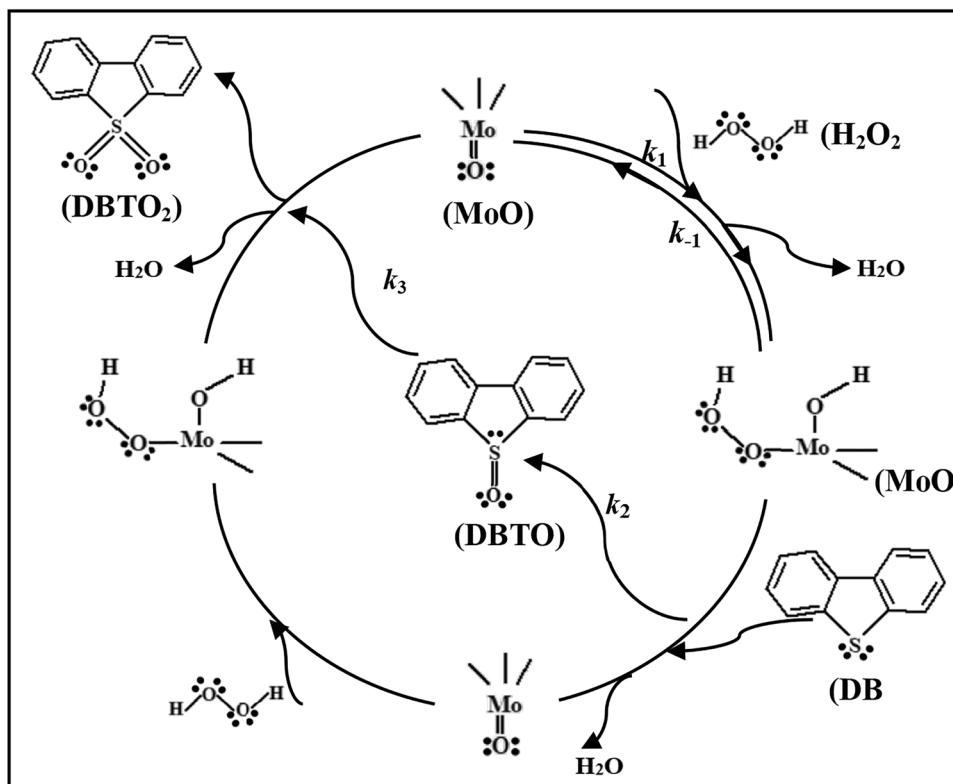
Equation (9) can be written in the form of Eq. (14) by using Eq. (13):

$$\begin{aligned} -r_{\text{DBT}} &= \frac{dC_{\text{DBT}}^S}{dt} = k_2 C_{\text{DBT}}^S C_{\text{MoO}_2} \\ &= \frac{k_1 C_{\text{Mo}} C_{\text{H}_2\text{O}_2} k_2 C_{\text{DBT}}^S}{k_{-1} + k_2 C_{\text{DBT}}^S + k_1 C_{\text{H}_2\text{O}_2} + k_3 C_{\text{DBTO}_2}^S} \end{aligned} \tag{14}$$

At initial conditions, the third step of the reaction would be negligible and Eq. (14) can be obtained as follows:

$$-r_{\text{DBT}}^0 = \frac{dC_{\text{DBT}}^S}{dt} = \frac{k_1 C_{\text{Mo}} C_{\text{H}_2\text{O}_2}^0 k_2 C_{\text{DBT}}^S}{k_{-1} + k_2 C_{\text{DBT}}^S + k_1 C_{\text{H}_2\text{O}_2}^0} \tag{15}$$

Fig. 8 Schematics of the oxidation reaction sequence



Considering the control step of the reaction mechanism:  $k_{-1} + k_1 C_{H_2O_2} \gg k_2 C_{DBT}^S$  and Eq. (15) can be simplified to Eq. (16):

$$-r_{DBT} = \frac{dC_{DBT}^S}{dt} = \frac{k_1 C_{Mo} C_{H_2O_2} k_2 C_{DBT}^S}{k_{-1} + k_1 C_{H_2O_2}} \tag{16}$$

Equation (16) suggests a linear relationship between  $C_{DBT}^S$  and  $t$  (a first order oxidation rate) as follows:

$$-r_{DBT} = K_r C_{DBT}^S \tag{17}$$

in which,  $K_r = \frac{k_1 C_{Mo} C_{H_2O_2} k_2}{k_{-1} + k_1 C_{H_2O_2}}$ .

Therefore, the catalytic oxidative desulfurization can be treated as a pseudo-first-order reaction. Within the extraction-oxidation steady state conditions, the mass balance of DBT can be written as:

$$J_{DBT}^F = J_{DBT}^E = J_{DBT}^S = -r_{DBT} \tag{18}$$

By inserting Eqs. (5), (6), (7), (8), and (17) in Eq. (18), the overall ECOD rate can be simplified as:

$$-r_{DBT} = K_r' C_{DBT}^F \tag{19}$$

where

$$K_r' = \frac{1}{\frac{1}{k_F a_L} + \frac{1}{k_E K_D a_L} + \frac{1}{K_D a_S k_S} + \frac{1}{K_D K_r}} \tag{20}$$

In the case of fast catalytic oxidation reaction when the extraction is the rate controlling step, the DBT concentration is expected to be close to zero in the extracting phase. However, based on the GC analysis of the two phases (Fig. 6b), DBT is present in the extracting phase during the whole process.

Therefore, it can be concluded that the extraction is not the rate controlling step and the ECOD rate is determined by catalytic oxidation. This is particularly true considering the flat structure of the 2D graphenic support applied in the present research that promotes the mass transfer rate and eliminates the pore penetration resistance [17]. The overall rate equation can be then simplified as:

$$-r_{DBT} = k_D K_r C_{DBT}^F = K_r'' \tag{21}$$

### 3.7.3 Kinetic Parameters

To obtain the kinetic parameters, the desulfurization experiments were carried out at different temperatures of 298, 313, 323, and 333 K. As seen in Fig. 9a, the temperature plays a significant role in the performance of the ECOD process. The sulfur removal is low at the lowest temperature (32.8%)

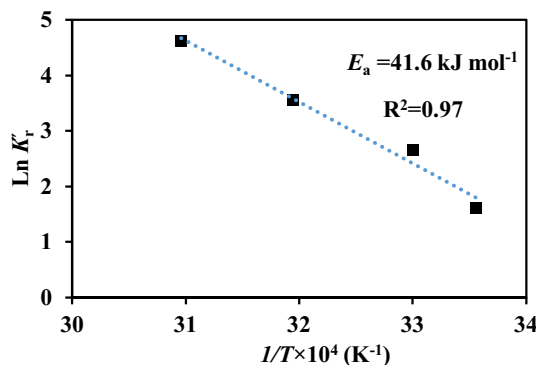


Fig. 10 Arrhenius activation energy for oxidation of DBT. Experimental conditions:  $T=50\text{ }^\circ\text{C}$ , Catalyst ( $Mo_{12}$ -GO) loading:  $2.4\text{ g L}^{-1}$ , O/S=6, extracting solvent: acetonitrile, E/F=0.3, sulfur containing compound: DBT, and 30-min run

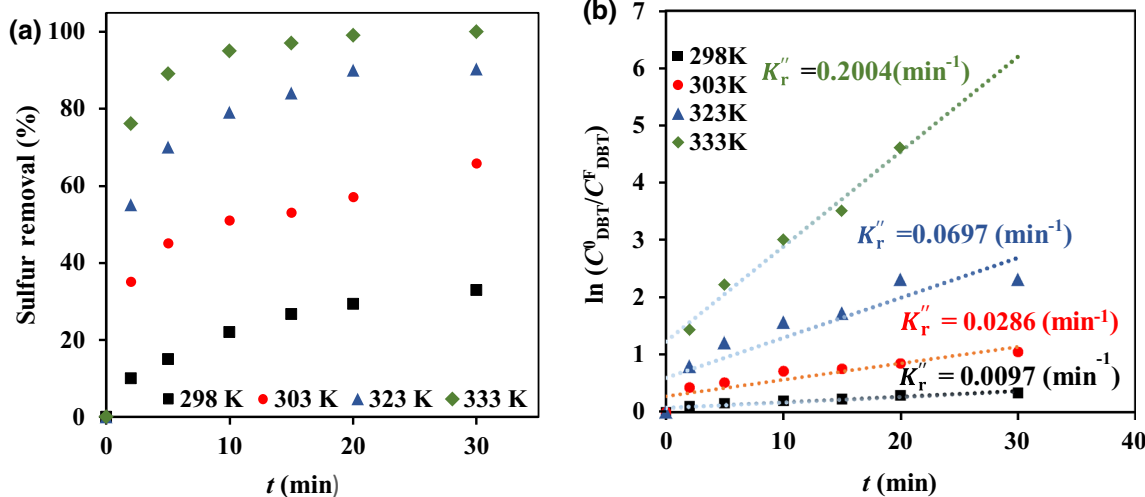


Fig. 9 (a) Temperature dependence, and (b) pseudo-first-order kinetic plots for ECOD process; Experimental conditions:  $T=50\text{ }^\circ\text{C}$ , Catalyst ( $Mo_{12}$ -GO) loading:  $2.4\text{ g L}^{-1}$ , O/S=6, extracting solvent: acetonitrile, E/F=0.3, sulfur containing compound: DBT, and 30-min run

while it increases to 65.7%, 90.2%, and 100% upon increasing the temperature to 313, 323, and 333 K, respectively. The values of the apparent reaction rate constant,  $K_r''$ , were calculated based on the plot of  $\ln\left(\frac{C_{DBT}^F}{C_{DBT}^O}\right)$  against the reaction time (Fig. 9b). According to the fig, the rate constants  $K_r''$  increase with increasing the reaction temperature, which implies that the total resistance decrease by increasing the reaction temperature. The corresponding Arrhenius plot is represented in Fig. 10 and the apparent activation energy is determined as  $41.6 \text{ kJ mol}^{-1}$ , which is in agreement with other reports on HPAs desulfurization processes [4, 15, 44].

## 4 Conclusion

A series of HPA-GOs catalysts consisting of W and Mo were prepared, characterized, and utilized for desulfurization of BT, DBT, and 4,6-DMBT in the ECOD process. The effective parameters such as the types of catalyst and extracting solvent, calcination of catalyst, and initial sulfur concentration were investigated and a two-phase kinetic model was developed. According to the results, the desulfurization efficiency was gradually increased for all sulfur containing compounds with increasing the molybdenum ions in the catalyst so that the calcined  $\text{Mo}_{12}$ -GO catalyst showed the complete removal of DBT as well as 4,6-DMBT within the 30 min. Among different extracting solvents, NMP exhibited the best extractive desulfurization performance and acetonitrile showed the best ECOD desulfurization performance due to its physiochemical properties. Although, the intermediate ECOD performance of non-calcined catalyst was slightly higher than that by the calcined one due to presence of surface oxygen containing groups, the more stable calcined catalyst was adopted for the whole experiments. The ECOD process represented high sulfur removals (100% and 97.5%) for the feeds with 500 and 1000 ppm sulfur concentration, respectively.

Mass transfers in the phases were studied and a kinetic model considering mass transfer coupling with chemical reaction was developed that could well predict the experimental data as a pseudo-first order kinetic model. The chemical reaction step was recognized as the rate controlling step in the ECOD system and the apparent reaction activation energy was determined as  $41.6 \text{ kJ mol}^{-1}$ . The fast performance of ECOD process with the HPA-GO catalysts may partly be attributed to the nonporous 2D structure of the catalyst, which promotes the mass transfer rate and eliminates the penetration resistance during the reaction.

## Compliance with Ethical Standards

**Conflict of interest** All authors declare no conflicts of interest.

## References

- Komintarachat C, Trakarnpruk W (2006) Oxidative desulfurization using polyoxometalates. *Ind Eng Chem Res* 45:1853–1856
- Otsuki S, Nonaka T, Takashima N et al (2000) Oxidative desulfurization of light gas oil and vacuum gas oil by oxidation and solvent extraction. *Energy Fuels* 14:1232–1239
- Chamack M, Mahjoub AR, Aghayan H (2014) Cesium salts of tungsten-substituted molybdophosphoric acid immobilized onto platelet mesoporous silica: efficient catalysts for oxidative desulfurization of dibenzothiophene. *Chem Eng J* 255:686–694
- Wang R, Zhang G, Zhao H (2010) Polyoxometalate as effective catalyst for the deep desulfurization of diesel oil. *Catal Today* 149:117–121
- Lu Y, Liu M, Nie H et al (2016) Direct fabrication of metal-free hollow graphene balls with a self-supporting structure as efficient cathode catalysts of fuel cell. *J Nanopart Res* 18:141–156
- Khodadadi DA, Mortaheb HR, Mokhtarani B (2018) Complete oxidative desulfurization using graphene oxide-based phosphomolybdic acid catalyst: process optimization by two phase mass balance approach. *Chem Eng J* 335:362–372
- Maity U, Basu JK, Sengupta S (2014) Performance study of extraction and oxidation—extraction coupling processes in the removal of thiophenic compounds. *Fuel Process Technol* 121:119–124
- Suryawanshi NB, Bhandari VM, Sorokhaibam LG et al (2016) A non-catalytic deep desulphurization process using hydrodynamic cavitation. *Sci Rep* 6:1–8
- Suryawanshi NB, Bhandari VM, Sorokhaibam LG et al (2017) Developing techno-economically sustainable methodologies for deep desulfurization using hydrodynamic cavitation. *Fuel* 210:482–490
- De Filippis P, Scarsella M (2003) Oxidative desulfurization: oxidation reactivity of sulfur compounds in different organic matrixes. *Energy Fuels* 17:1452–1455
- Lu Z, Guo E, Zhong H et al (2016) Kinetic modeling of the extraction–oxidation coupling process for the removal of dibenzothiophene. *Energy Fuels* 30:7214–7220
- Haw KG, Abu bakar WAW, Ali R et al (2010) Catalytic oxidative desulfurization of diesel utilizing hydrogen peroxide and functionalized-activated carbon in a biphasic diesel-acetonitrile system. *Fuel Process Technol* 91:1105–1112
- Yang H, Jiang B, Sun Y et al (2017) Heterogeneous oxidative desulfurization of diesel fuel catalyzed by mesoporous polyoxometallate-based polymeric hybrid. *J Hazard Mater* 333:63–72
- Tian Y, Yao Y, Zhi Y et al (2015) Combined extraction-oxidation system for oxidative desulfurization (ODS) of a model fuel. *Energy Fuels* 29:618–625
- Sengupta A, Kamble PD, Basu JK et al (2012) Kinetic study and optimization of oxidative desulfurization of benzothiophene using mesoporous titanium silicate-1 catalyst. *Ind Eng Chem Res* 51:147–157
- Okuhara T, Mizuno N, Misono M (1996) Catalytic chemistry of heteropoly compounds. *Adv Catal* 41:113–252
- Fan X, Zhang F (2015) Multiple roles of graphene in heterogeneous catalysis. *Chem Soc Rev* 44:3023–3035
- Zhang Y, Wang R (2017) Nanocarbon materials for oxidative-adsorptive desulfurization using air oxygen under mild conditions. *Diam Relat Mater* 73:161–168
- Menzel R, Iruretagoyena D, Wang Y et al (2016) Graphene oxide/mixed metal oxide hybrid materials for enhanced adsorption desulfurization of liquid hydrocarbon fuels. *Fuel* 181:531–536
- Hajjar Z, Kazemeini M, Rashidi A et al (2016) Graphene based catalysts for deep hydrodesulfurization of naphtha and diesel fuels: a physiochemical study. *Fuel* 165:468–476

21. Khodadadi Dizaji A, Mortaheb HR, Mokhtarani B (2017) Preparation of supported catalyst by adsorption of polyoxometalate on graphene oxide/reduced graphene oxide. *Mater Chem Phys* 199:424–434
22. Khodadadi Dizaji A, Mortaheb HR, Mokhtarani B (2017) Per-vaporative performance of polydimethylsiloxane–graphene/polyethersulfone hybrid membrane: effects of graphene structure and surface properties. *Chem Eng Res Des* 124:181–192
23. Marcano D, Kosynkin D, Berlin J (2010) Improved synthesis of graphene oxide. *ACS Nano* 4:4806–4814
24. Chamack M, Mahjoub AR, Aghayan H (2015) Catalytic performance of vanadium-substituted molybdophosphoric acid supported on zirconium modified mesoporous silica in oxidative desulfurization. *Chem Eng Res Des* 94:565–572
25. Lu H, Ren W, Wang H et al (2013) Deep desulfurization of diesel by ionic liquid extraction coupled with catalytic oxidation using an Anderson-type catalyst [(C<sub>4</sub>H<sub>9</sub>)<sub>4</sub>N]<sub>4</sub>NiMo<sub>6</sub>O<sub>24</sub>H<sub>6</sub>. *Appl Catal A Gen* 453:376–382
26. Shen D, Dai Y, Han J et al (2017) A nanocellulose template strategy for the controllable synthesis of tungsten-containing mesoporous silica for ultra-deep oxidative desulfurization. *Chem Eng J* 332:563–571
27. De Angelis A, Pollesel P, Molinari D et al (2007) Heteropolyacids as effective catalysts to obtain zero sulfur diesel. *Pure Appl Chem* 79:1887–1894
28. Choi AES, Roces S, Dugos N et al (2016) Oxidation by H<sub>2</sub>O<sub>2</sub> of bezothiophene and dibenzothiophene over different polyoxometalate catalysts in the frame of ultrasound and mixing assisted oxidative desulfurization. *Fuel* 180:127–136
29. Sobati MA, Dehkordi AM, Shahrokhi M (2010) Extraction of oxidized sulfur-containing compounds of non-hydrotreated gas oil. *Chem Eng Technol* 33:1515–1524
30. Ramírez-Verduzco LF, Torres-García E, Gómez-Quintana R et al (2004) Desulfurization of diesel by oxidation/extraction scheme: influence of the extraction solvent. *Catal Today* 98:289–294
31. Zhao K, Cheng Y, Liu H et al (2015) RSC Advances extractive desulfurization of dibenzothiophene by a optimization by Box—Behnken design. *RSC Adv* 5:66013–66023
32. Tegou E, Pseiropoulos G, Filippidou MK et al (2016) Low-temperature thermal reduction of graphene oxide films in ambient atmosphere: infra-red spectroscopic studies and gas sensing applications. *Microelectron Eng* 159:146–150
33. Gu Q, Wen G, Su D (2017) Reduced graphene oxide: a metal-free catalyst for aerobic oxidative desulfurization. *Green Chem* 19:1175–1181
34. Katheria S, Gupta A, Deo G et al (2016) Effect of calcination temperature on stability and activity of Ni/MgAl<sub>2</sub>O<sub>4</sub> catalyst for steam reforming of methane at high pressure condition. *Int J Hydrog Energy* 41:14123–14132
35. Wang R, Yu F, Zhang G et al (2010) Performance evaluation of the carbon nanotubes supported Cs<sub>2.5</sub>H<sub>0.5</sub>PW<sub>12</sub>O<sub>40</sub> as efficient and recoverable catalyst for the oxidative removal of dibenzothiophene. *Catal Today* 150:37–41
36. García-Gutiérrez JL, Fuentes GA, Hernández-Terán ME et al (2008) Ultra-deep oxidative desulfurization of diesel fuel by the Mo/Al<sub>2</sub>O<sub>3</sub>–H<sub>2</sub>O<sub>2</sub> system: the effect of system parameters on catalytic activity. *Appl Catal A Gen* 334:366–373
37. Qin L, Zheng Y, Li D et al (2016) Phosphotungstic acid immobilized on amino functionalized spherical millimeter-sized mesoporous Al<sub>2</sub>O<sub>3</sub> bead and its superior performance in oxidative desulfurization of dibenzothiophene. *Fuel* 181:827–835
38. Azu KY, Uruya TF, Iki KM (2003) Immobilized tungstophosphoric acid catalyzed oxidative desulfurization of diesel oil with hydrogen peroxide. *J Jpn Petroleum Inst* 46:379–382
39. Ribeiro S, Barbosa ADS, Gomes AC et al (2013) Catalytic oxidative desulfurization systems based on Keggin phosphotungstate and metal-organic framework MIL-101. *Fuel Process Technol* 116:350–357
40. Ertl G, Knözinger H, Schüth F et al (2008) *Handbook of heterogeneous catalysis*, 2nd edn. Wiley-VCH, Weinheim
41. Khodadadi Dizaji A, Mortaheb HR, Mokhtarani B (2016) Non-covalently functionalized graphene oxide / graphene with imidazolium-based ionic liquids for adsorptive removal of dibenzothiophene from model fuel. *J Mater Sci* 51:10092–10103
42. Dumitriu E, Guimon C, Cordoneanu A et al (2001) Heterogeneous sulfoxidation of thioethers by hydrogen peroxide over layered double hydroxides as catalysts. *Catal Today* 66:529–534
43. Zhu W, Li H, Gu Q et al (2011) Kinetics and mechanism for oxidative desulfurization of fuels catalyzed by peroxo-molybdenum amino acid complexes in water-immiscible ionic liquids. *J Mol Catal A Chem* 336:16–22
44. Zhu W, Zhu G, Li H et al (2013) Catalytic kinetics of oxidative desulfurization with surfactant-type polyoxometalate-based ionic liquids. *Fuel Process Technol* 106:70–76

## Affiliations

Azam Khodadadi Dizaji<sup>1</sup> · Hamid Reza Mortaheb<sup>1</sup> · Babak Mokhtarani<sup>1</sup>

✉ Hamid Reza Mortaheb  
mortaheb@ccerci.ac.ir

✉ Babak Mokhtarani  
mokhtarani@ccerci.ac.ir

<sup>1</sup> Chemistry and Chemical Engineering Research Center of Iran, P.O. Box 14335-186, Tehran, Iran